Journal of Materials Research and Technology 33 (2024) 5543–5550

Contents lists available at ScienceDirect

Journal of Materials Research and Technology

journal homepage: www.elsevier.com/locate/jmrt

Silicone rubber nanocomposites: Optimal graphene dosing for mechanical and electrical enhancements

Vishal Deore [a,b], Milinda Mahajan [a], I. Siva [c], Avinash Shinde [b], Smita Waghmare [d], Sharul Sham Dol [e], K.A. Ahmad [f], Mohamed Thariq Hameed Sultan [g,h,*]

[a] Department of Technology, Savitribai Phule Pune University, Pune, MH, India
[b] Cummins College of Engineering for Women, Pune, MH, India
[c] Department of Mechanical Engineering, Mohan Babu University, Tirupati, 517102, AP, India
[d] Nowrosjee Wadia College, Pune, MH, India
[e] Mechanical and Industrial Engineering Department, Abu Dhabi University, PO Box, 59911, Abu Dhabi, United Arab Emirates
[f] Department of Aerospace Engineering, Faculty of Engineering, Universiti Putra Malaysia, 43400, Serdang, Selangor, Malaysia
[g] Laboratory of Biocomposite Technology, Institute of Tropical Forestry and Forest Products, Universiti Putra Malaysia, 43400, Serdang, Selangor, Malaysia
[h] Aerospace Malaysia Innovation Centre (944751-A), Prime Minister's Department, MIGHT Partnership Hub, Jalan Impact, Cyberjaya, 63000, Malaysia

ARTICLE INFO

Handling editor: M Meyers

Keywords:
Silicon rubber (SR)
Graphene
Copper oxide (CuO)
Mechanical properties

ABSTRACT

The combination of lightweight, durable, and flexible elastomer nanocomposites presents a unique set of features that make them highly promising for a range of several engineering applications. Present work investigates the performance of the mechanical and electrical characteristics of a nanocomposite produced by combining silicon rubber (SR) with nano-Graphene, copper oxide (CuO). Two roll mixing followed by compression moulding is used to manufacture different configurations of Graphene/CuO/SR nano composite. Nano composites specimens are fabricated with 1, 2, 4, and 8 wt % of graphene with fixed 1 % CuO. There has been a discernible improvement of 146.52 % in the mechanical properties and 18.1 % in electrical performance. This improvement is supported by the FESEM morphological analysis of fractured surfaces. It has been observed that the optimized loading of 8 wt % of Graphene gives the best performance. The strong interfacial interaction between the Graphene/CuO and SR is responsible for the performance gain.

1. Introduction

Silicone rubber, (SR) a versatile elastomer, finds applications across various industries due to its unique properties, including flexibility, heat resistance, chemical stability, and biocompatibility. The common applications of silicone rubber are as a sealants and gaskets, du tot its ability to withstand extreme temperatures, weathering, and UV radiation It is also popular in automotive, construction, and aerospace industries. Silicone rubber is widely used in medical devices and equipment such as tubing, implants, prosthetics, and catheters due to its biocompatibility, flexibility, and resistance to sterilization methods.

Ahmed Thabet and Fahad A. Al Mufadi [1] explores advancements in the optical characterization of nanostructures composed of single-walled (SR) and multi-walled carbon nanotubes (MWCNTs). These nanostructures hold promise for use in emerging piezoelectric sensors. The author emphasizes potential applications of SR/MWCNTs in the development of highly sensitive piezoelectric sensors. While Guangzhi Jin et al. [2], presents a technique for producing fluorescent silicon rubber. The method involves melt-compounding silicon rubber with a crude fluid containing carbon dots. The resulting fluorescent silicon rubber holds potential for various applications due to its unique optical properties. The feasibility of using silicon rubber membrane extraction to recover o-toluidine and p-toluidine from wastewater investigated by Chao Zhu et al. [3]. Liangqing Lai et al. [4] provides a concise overview of recent developments in flame retardant rubber composites. The short review discusses advancements in enhancing the flame retardancy of rubber composites through various approaches, such as incorporating flame retardant additives, nanomaterials, and synergistic combinations. Atefeh Heidarian et al., [5,7] investigates nickel-coated graphite/silicone rubber composites for their potential

* Corresponding author. Laboratory of Biocomposite Technology, Institute of Tropical Forestry and Forest Products, Universiti Putra Malaysia, 43400, Serdang, Selangor, Malaysia.
E-mail address: thariq@upm.edu.my (M.T.H. Sultan).

https://doi.org/10.1016/j.jmrt.2024.10.206
Received 17 September 2024; Received in revised form 21 October 2024; Accepted 23 October 2024
Available online 24 October 2024

application as electromagnetic interference (EMI) shielding gaskets. The study explores the fabrication process and characterizes the electromagnetic interference shielding effectiveness of the composites for various engineering application. The manufacturing and characterization of hydrophobic surface, including water contact angle and durability and its applications in various fields, such as self-cleaning coatings and water-repellent materials is also studied [6,22].

One of the study explores the effects of boron nitride nanosheets on improving the thermal conductivity and electrical insulation properties of silicone rubber nanocomposite, highlighting their potential applications in various industries, including electronics and automotive, wearable electronics and biomedical devices, flexible capacitive sensor [8–10]. The impact of graphite and polyetherimide (PEI)-coated silicon rubber for enhancing the rheological, morphological, and thermomechanical properties of composites comprising polyetherimide and liquid crystalline polymer is studied [11]. Pei Huang et al. [12,13,17], explores the 3D printing of carbon fiber-filled conductive silicon rubber for electrical and mechanical performance. Thermal conductivity of silicone rubber composites, which is crucial for applications requiring efficient heat dissipation, such as electronic devices, and frozen foods packaging is studied [14,15]. The effect [16,18,20] of ultrafine Al_2O_3 nanospheres, aluminium nitride (AlN) using Polysilazane and the amorphous silicon oxycarbide on ceramic composite for improvement in mechanical and thermal conductivity is studies [16,18–20]. Through various characterization techniques, including surface morphology and chemical composition analysis, the effects of plasma treatment on the surface properties of silicon rubber are elucidated, providing valuable insights into surface modification techniques for enhancing material performance. The study [21] investigates the effects of graphene dosage on the friction and wear performance of a graphene-reinforced silicone rubber nanocomposite, The author [23,24] presents a novel aging characterization method for silicone rubber using terahertz absorption spectroscopy. The Jingchao Li et al. [25] demonstrates the effectiveness of the foams in providing EMI shielding and high thermal conductivity, offering potential applications in electronics and thermal management systems [26].

Plentiful literature is available on the silicon rubber composite. To best of authors knowledge no work explores the mechanical and electrical performance of silicon rubber reinforced with graphene nanofillers and copper oxide. Considering the versatility of silicon rubber, the study is beneficial for the research community in the field of rubber nanocomposite.

2. Materials and methods

2.1. Material

In this research, the silicon rubber (SR) grade SH5060U a major constituent is supplied by Krupa Chemicals, Pune, India along with the peroxide-based accelerator Dicup-40 (DCP). 99% pure graphene has a length of 10 nm is supplied by Shimoga (Ad-Nano Technologies Private Limited), Bangalore, India. Copper Oxide (CuO), with a purity of 99% is supplied by Shimoga, Bangalore, India with an average size of particle <100 nm. The molecular weight of CuO is 101.96 g/mol having melting point of 1326 °C and the surface area as 60–80 m^2/g, bulk density 0.9 g/cm^3. Table 1 presents the basic properties of SR and two different fillers.

Table 1
Materials Description.

Type/Grade	Silicon Rubber (SR)	Graphene	Copper Oxide
Hardness, shore	50 (A)	70 HRC	4 (Mohs Scale)
Elongation (%)	500	5	1
Tensile strength Ultimate	5.5 MPa	132 GPa	200 MPa
Specific Gravity (g/cc)	1.16	1.6	5.5

2.2. Composite manufacturing

Table 2 presents the compositions of nano filler and curing agent used with Silicon Rubber in composite manufacturing. Nano-Graphene of weight percentage ranging from 1 to 8% is mixed with SR to form targeted composites. CuO wt. % is maintained as 1 in all the nanocomposite manufacturing. Di-Cup 40 (Dicumyl peroxide – DCP OF 2%) used as a curing (cross-linking) agent compound. The blend of each composite with these three constituents and Di-Cup 40 is fed to two roll milling unit for comprehensive blending for 20 min followed by the hot compression [29,30,33]. The blend is pressed for 50 Bar for 5 min at 180 °C. A hot-air oven was used for curing during at the end at 200 °C for 4 h. Fig. 1 illustrate the complete process of manufacturing.

2.3. Characterisations

2.3.1. Mechanical studies of composites

Various techniques are utilized to investigate how filler and hybridization affect the fundamental mechanical characteristics of the composites that are created. Uniaxial tensile properties are examined following the guidelines of ASTM D412. Experiments were carried out using a 450 mm/min strain rate. The ASTM D2240 guidelines were followed in measuring the shore hardness. The experiments were conducted at the standard temperature. Examining the fractured surface of the composite samples involved utilizing an FEI Nova NanoSEM 450 device for ultra-high resolution (FEI, Hillsboro, OR USA). Additionally, the SR and hybrid composites were analyzed using an XRD instrument (Rigaku Miniflex 600 XRD) Using Cu K radiations (=0.154 nm) in X-rays and a dispersion angle theta ranging from 20^o to 80^o. Fig. 2 shows the sized and fractured samples after various examinations.

2.3.2. Electrical conductivity measurements

Fig. 3 illustrates the experimental procedure of the measuring the electrical conductivity of the fabricated composites. Specimen were prepared by sizing the fabricated composites into 150 mm × 150 mm size samples. The insulation testers' application of the insulation-resistance measurement principle. By measuring the current, I that flows to the target when the voltage V is applied and dividing the applied voltage V by the resultant current I, one can determine the insulation resistance Rx of the measurement target.

3. Result and discussion

3.1. Mechanical characteristics

3.1.1. Variation in hardness

In accordance with ASTM D2240 shore A inspection, each and every produced SR and nano-hybrid composite is given a thorough examination. In Fig. 4, we see an illustration of the variation in shore A hardness that occurs as a function of filler loading on the SR matrix. The increase in packing density and load bearing capability of the base material will be resulted due to the significant rise in the hardness of the material. When compared to the other composites that were investigated, the neat SR had the lowest hardness (68 shore A). With the addition of graphene

Table 2
Weight Percentage of nano Filler and curing Agent.

Sample No	Silicon Rubber (gms)	% of Graphene	Graphene Qty (in gms)	% of CuO	CuO Qty (in gms)	DCP (%)
SR1	1000	0	0	0	0	2
SR2	1000	0	0	1	10	2
SR3	1000	1	10	1	10	2
SR4	1000	2	20	1	10	2
SR5	1000	4	40	1	10	2
SR6	1000	8	80	1	10	2

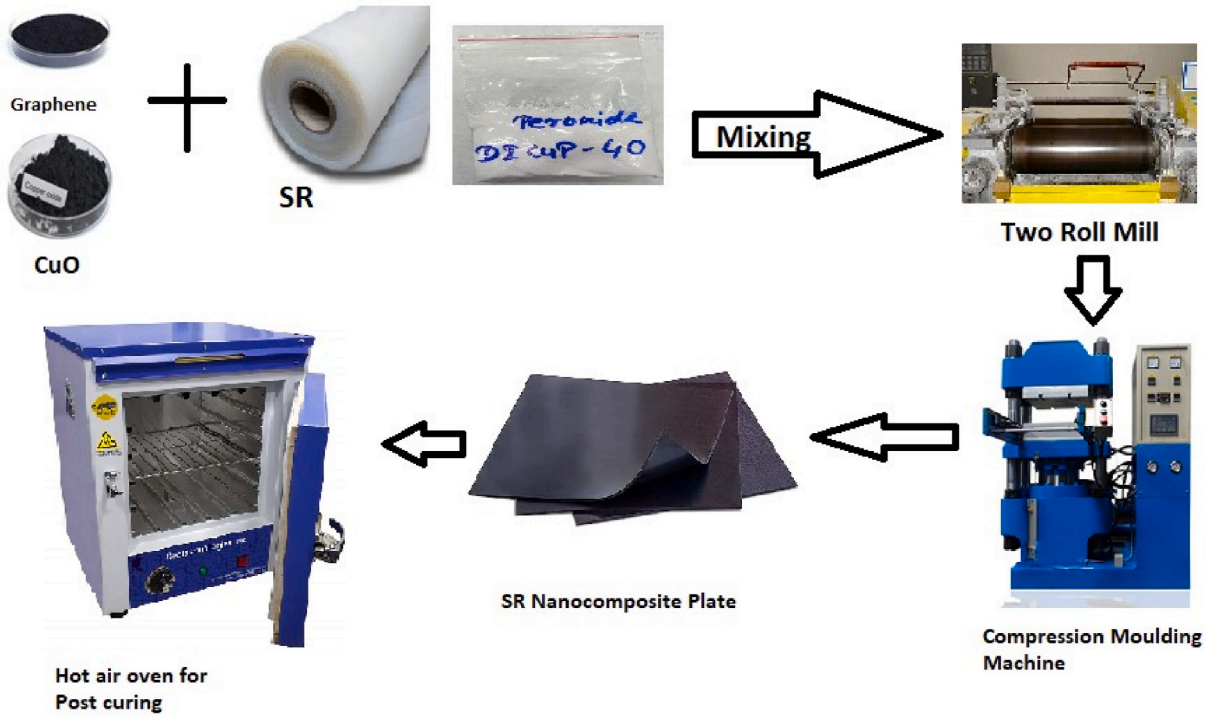

Fig. 1. Schematic process of Silicon rubber (SR) nanocomposite manufacturing.

Fig. 2. Images of fabricated and tested samples.

and CuO at a concentration of 1% into the SR base, there was a noticeable increase in hardness of around 2%. In addition, a linear increase is observed in conjunction with the additional increase in the hybridization of the SR base component. When contrasted with the other composites, the 8% hybrid SR composite exhibits a substantially higher increase in hardness than the other composites [31].

To be more specific, the dispersion strengthening of the SR that occurs as a result of the hybrid fillers attributing the first increase in hardness that occurs because of the inclusion of fillers. In the course of their interactions with the SR at the molecular level, the fillers brought about considerable alterations in the intermolecular packing density. When the hybridization was increased even further, the SR base became even more harder to uphold the mechanical loading. On the other hand, the density of the neat and hybrid SR composites linearly rises with the increase in the filler loading on the SR foundation.

3.1.2. Tensile strength

Adding the nanofillers into silicone rubber matrix significantly

Fig. 3. Electrical Conductivity Line diagram of Silicon Rubber Composite.

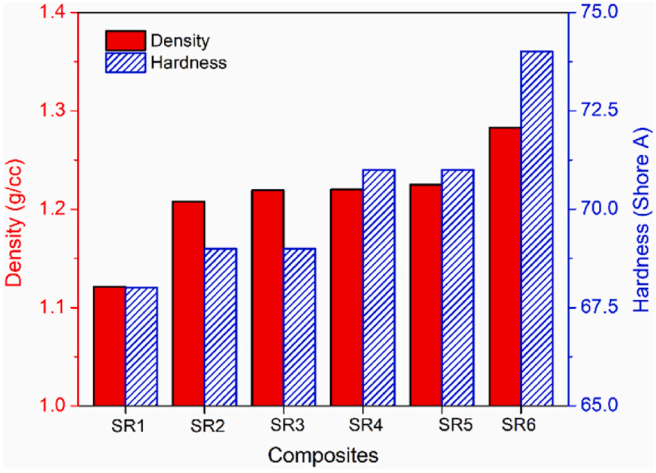

Fig. 4. Function of filler concentration on the hardness and density.

enhances its tensile strength by altering the load transfer, crack bridging and deflection, interfacial interactions, filler hierarchal network formation, and achieving uniform dispersion (Fig. 5) and improved stress transfer ability [27]. These mechanisms work together to create a material with the ability to endure greater tensile stresses and enhance its overall mechanical performance. The neat form of cured rubber matrix possesses 3.59 MPa tensile strength. Nanofillers serve as strengthening agents that limit the movement of the silicone rubber chains. This limitation results in a higher modulus and tensile strength. By creating a network within the rubber matrix, the fillers assist in evenly distributing the applied load across the material. A linear correlation found between the weight of fillers added and tensile strength of the rubber composites. However, the increment is not significant until SR5. The tensile strength of 1% dosed nanocomposite (SR2) rose to 3.65 MPa. Comparably, the measurements for SR3 and SR4 were 3.82 MPa and 3.92 MPa, respectively. With a strength of 5.29 MPa, the composition of SR5 is 146.52% stronger than pure SR. The addition of rigid inorganic filler improves the tensile strength. Another reason for improvement in the strength is the surface area. Graphene nanopartilces having high surface area supports the efficient stress transfer mechanism [28]. When 5% fillers dosed silicone rubber nanocomposite is subjected to tensile loading, cracks

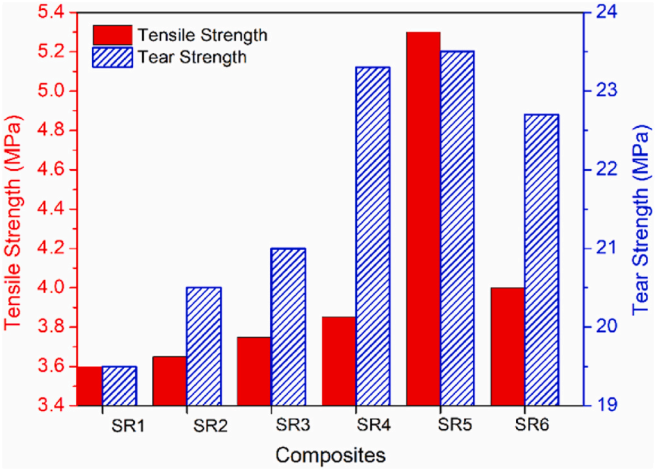

Fig. 5. Tensile Strength and tear strength of Silicon Rubber/Graphene/CuO Nanocomposite with weight % of nano fillers (Table 2).

would form; the addition of nanofillers can help to bridge these cracks and stop them from spreading. In addition, the nanofillers could deflect and blunt the cracks, which results in a higher energy requirement for crack propagation. This mechanism improves the tensile strength of the silicone rubber. Nevertheless, further dosing of nanofillers result-in clustering and rolling effects inside the matrix. Hence the nanocomposite with larger nanofillers incorporates weaker the material system. Poor interfacial adhesion also significantly affects the strength of particulate composite, although the filler wt. % is increased [28].

3.1.3. *Tear strength*

Overall, the incorporation of nanographene and CuO fillers into silicone rubber enhances its tear strength by improving stress transfer and load distribution, reinforcing, and toughening the material, bridging, and deflecting cracks, promoting strong interfacial interactions, forming a hybrid network, facilitating energy dissipation mechanisms, and achieving improved dispersion and distribution. These mechanisms work together to create a material that has excellent resistance to tearing, leading to better overall mechanical performance. In its pure form the cured silicon rubber holds 19.63 MPa tear strength (Fig. 5). Incorporation of 1% filler into the rubber significantly enhances the tear strength of the rubber composite. Due to the high aspect ratios and large surface areas, both the nanographene and CuO nanofillers enable effective stress transfer from the silicone matrix to the fillers. By distributing the applied loads more evenly throughout the material, the stress concentration at any point is reduced, resulting in improved tear resistance. In turn, the tear strength of the SR2 to SR5 composites recorded 20.05, 20.73 and 23.22 MPa respectively. Like tensile strength, the SR5 Nano-hybrid composites holds highest tear strength. Chemical groups nanofillers surface have strongly interact with the silicone chains can enhance the adhesion between the fillers and the matrix. The strong bonding at the interface enhances stress transfer and leads to enhanced mechanical characteristics, including increased tear resistance. Meanwhile, as its density rises, a greater increase in filler inclusion leads to the agglomeration of graphene and CuO. Consequently, as the mixture's graphene/CuO proportion increases, the adhesion between the components becomes unstable, hastening the SR nanocomposite's breakdown.

3.1.4. *Elongation at break, peak load, Braking load*

This shows how the concentration of Graphen/CuO affects the peak load and breaking load in Fig. 6. Among all the compositions, it is found that the SR5 composition has the maximum load-carrying capacity. Comparing the peak load to pure silicon rubber (SR1), there is a percentage improve of 162.19%, and the breaking load also shows an increase of SR3 Composition increases 128.9% of the same compare with

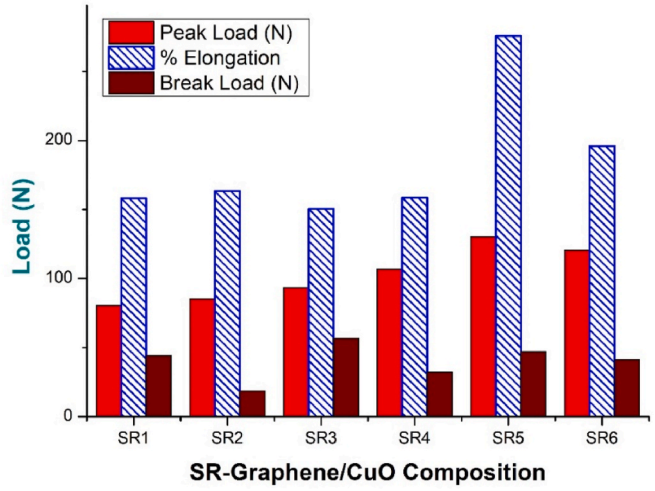

Fig. 6. Peak load, break load and % elongation at break for Silicon Rubber (SR) - Graphene/CuO Nano-composite.

pure SR (SR1). On the other hand, a decrease in the peak load and a 7.52% breaking load are noted with an additional concentration increase. These tendencies are caused by the SR and Graphene/CuO microstructure and interfacial bonding.

The % elongation at break [32] of the SR-Graphene/CuO nanocomposites for various compositions is displayed in Fig. 6. Up to a specific proportion, the percentage elongation at break rises as the Graphene/CuO concentration climbs. When comparing the SR5 composition to the SR1 composition, there is a 74.32% increase in elongation at break. The higher % elongation was a consequence of improved interlayer bonding for the SR5 composition. However, a further increase in the Graphene/CuO concentration results in a drop of 28.95%, which is explained by the Graphene/CuO particles aggregating in the matrix.

3.2. X-ray diffraction (XRD) studies

The X-ray diffraction graphs for the SR1, SR2, SR3, SR4, SR5, and SR6 samples are displayed in Fig. 7. The prominent peak values along with Intensity that appears of given specimen from SR1 to SR6 mentioned in Table 3. The peak at 28.686^0, however, indicates that the

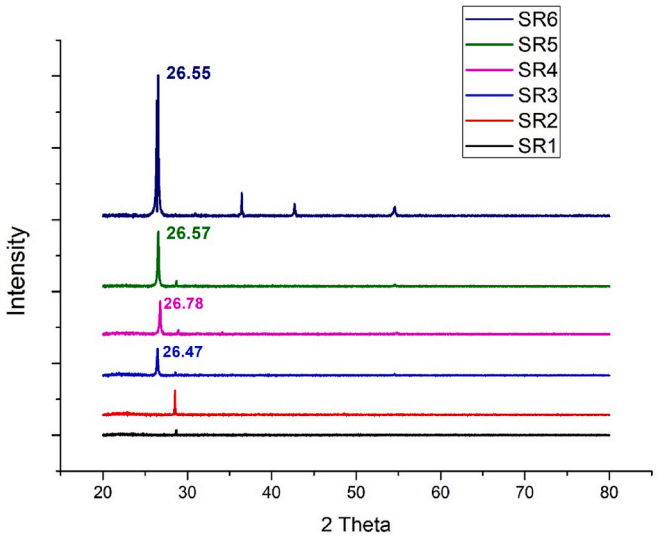

Fig. 7. XRD pattern of pure Silicon Rubber SR1, and Graphene/CuO matrix of SR2 to SR6 composition.

Table 3
XRD peak values (**2Θ**) with respective intensity of specimen from SR1 to SR6.

Specimen	SR1	SR2	SR3	SR4	SR5	SR6
Angle 2Θ (peak)	28.686	28.529	26.4710	26.784	26.568	26.549
Intensity	353	1687	1832	2285	3819	9775

peak's intensity is reduced to 2 theta angles of 26.784^0, 26.568^0, 26.549^0 when the data is analyzed using the SR4, SR5, SR6 composition respectively over intensity of 2285, 3819, 9775. The imposition of SR polymer molecules results in the development of a polymer composite reinforced with graphene/CuO, although it has no influence whatsoever on the crystalline structure of graphene/CuO.

A higher intensity of peaks often corresponds to a higher degree of crystallinity. This means that more of the material is organized into well-defined crystal structures, rather than being disordered. Whereas the crystallinity and structural properties of the material can also be inferred from the peak shapes. Broader peaks imply disorder or the existence of faults, whereas sharper peaks of SR3 to SR6 often indicate higher crystallinity and stronger organization.

3.3. Fracture surface field Emission Scanning electron microscopy (FE-SEM) analysis

After the specimens are first subjected to tensile testing, a FESEM analysis is performed to provide a rough understanding of the bonding between the graphene/CuO and the Silicon Rubber (SR). Fig. 8 displays a FESEM images of samples SR1–SR6's of failure surfaces of samples.

To give it a uniform appearance, The SR1 specimen is a smooth-polished piece of silicon rubber. The growing CuO and graphene/CuO density that has been found is clearly depicted in Fig. 8. This is demonstrated in Fig. 8. As the FESEM image demonstrates, a rise in graphene/CuO concentration causes the tensile and tear strengths of the SR3 composition to improve significantly. The increasing concentration of graphene/CuO is responsible for this improvement. If the FESEM image's uniform distribution and higher graphene/CuO content can justify further feature increases for the SR5 composition, then these same increases can also be supported by the composition itself. The FESEM picture shows that voids in the material caused cracks to emerge in the SR4. The observed decrease in the compositional properties of SR6 may be the result of these fissures.

This also alludes to the onset of graphene/CuO agglomeration, which happens when concentration increases The main cause of the appreciable improvement in the tensile characteristics that the nanocomposites exhibit is the enhanced adhesion between the matrix and the filler.

3.4. FTIR analysis

Fig. 9 displays the FTIR spectra for each potential combination of CuO/graphene and SR. These spectra demonstrate the distribution of silicone-containing groups. At wavenumbers between 500 and 1300 cm^{-1}, the fundamental functional group of SR can be seen in all data. The greatest values of Si–O–Si stretching, Si–O of O–Si(CH3)2–O, and Si–CH3 symmetry bending are 1,010, 789, and 1257 cm^{-1}, respectively. The presence of graphene causes a modest attenuation of the reported FTIR peak intensities [34]. The graphene barrier preventing the detection of Si chemical bonding in SR may account for this outcome. In addition to the Si bonds, it was found that every sample had a carboxyl group in the graphene molecule at wavenumber 1100 to 1500 cm^{-1}. Moreover, CuO exhibits peaks between 430 and 500 cm^{-1}.

3.5. EDS analysis

The EDS spectra displayed in Fig. 10 reveal the chemical composition of the fractured surface. In dry circumstances, silica, carbon, oxygen,

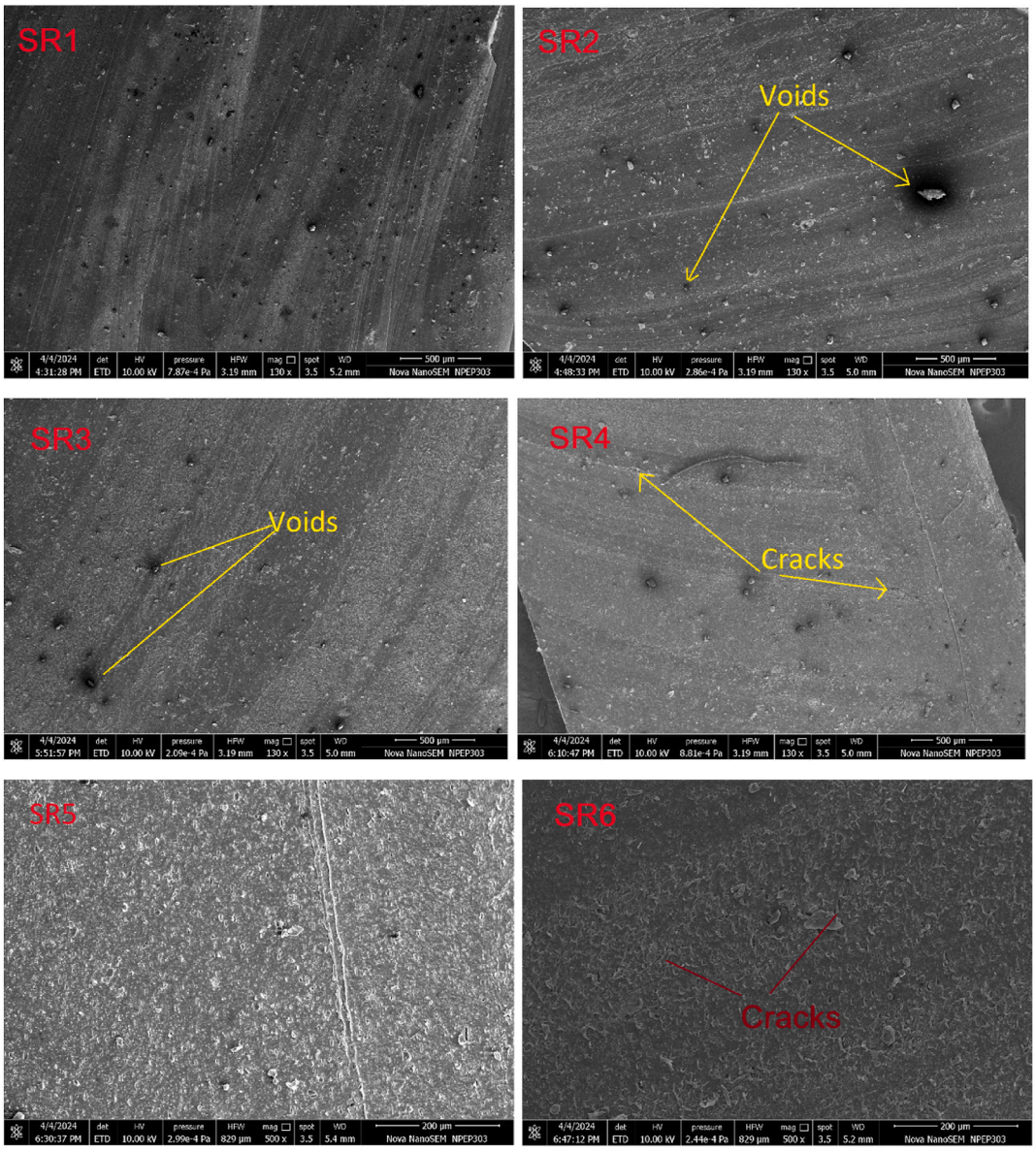

Fig. 8. Fracture Surface Morphology for SR1 to SR6 composition.

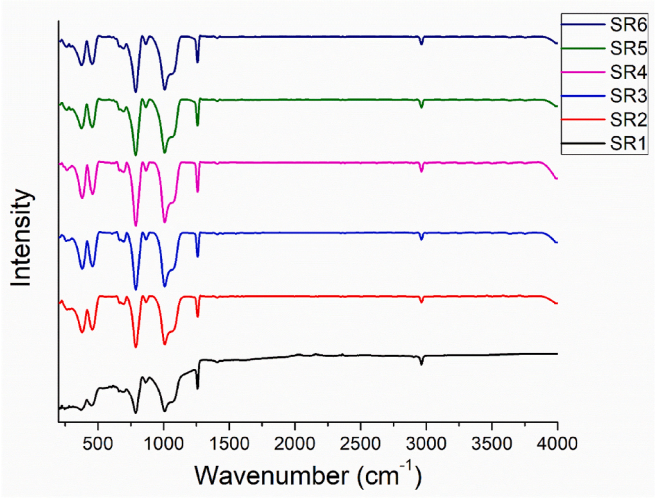

Fig. 9. FTIR spectrums of Silicon Rubber nanocomposite samples.

and copper are found on the fracture surface. Additionally, the weight percentages of O and C components in the SR5 composition are 31.76 and 28.79, respectively, whereas they are 32.73 and 27.89 in the SR6 composition.

More heat depolymerisation is evident in the SR6 compared to the SR5 composition, as seen by the higher count of the O element and lower count of the C element. However, specimens SR5 and SR6 had weight percentages of Cu elements of 0.9 and 0.94, respectively. Since the pure silicon rubber contains similar ingredients, it may be concluded that no chemical reaction occurred because of the specimen's breakage.

3.6. Electrical properties of SR composition

Electrical insulating applications are best suited for the high resistivity composite materials. As a result, (Tested under ASTM D 257) as illustrated in Table 4, the electrical resistivity of SR composite with various % wt filler were measured. Table 4 presents the exceptional electrical insulating qualities of pure SR composition, with resistivity up to >200GΩ. Nevertheless, after adding 1% weight percent Graphene, the composite film's volume electrical resistivity and clearly dropped. It

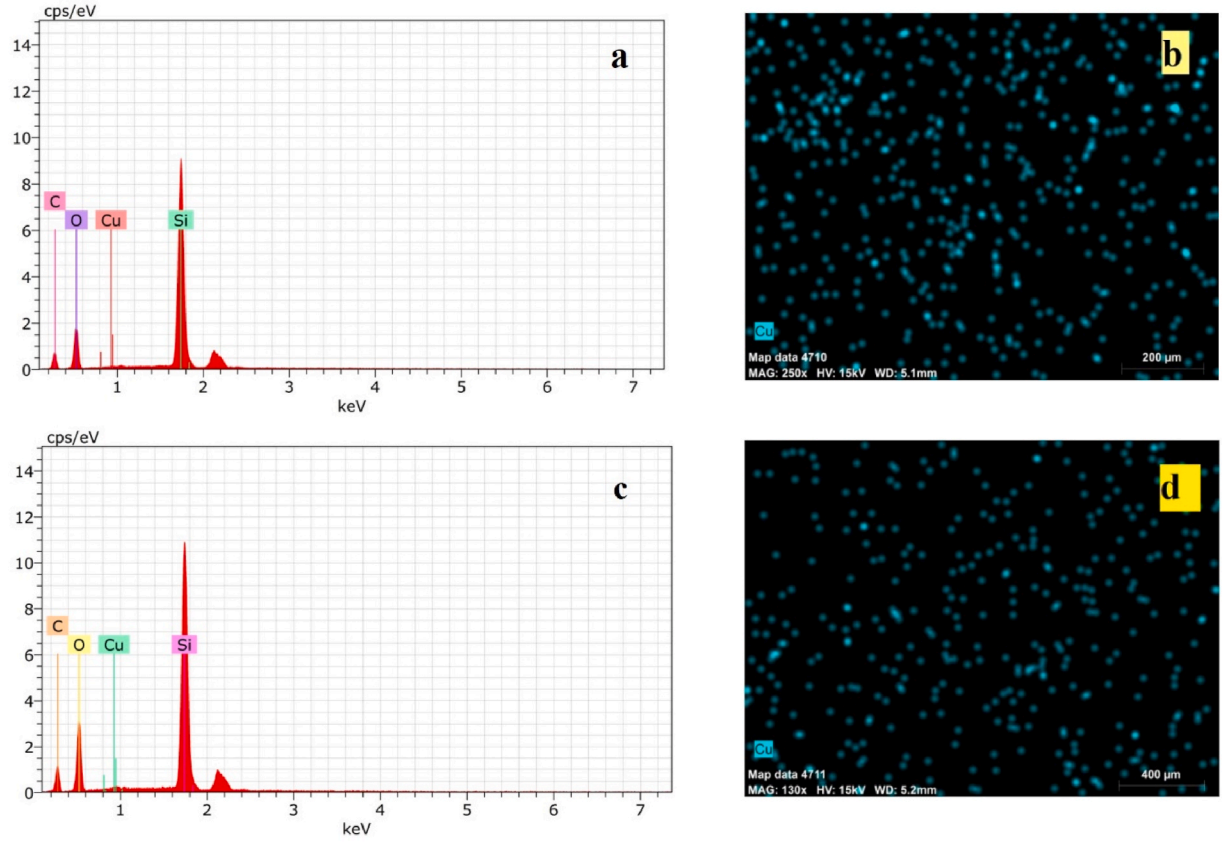

Fig. 10. (a) EDS Spectra and (b) Cu mapping monograph for SR5, and (c) EDS Spectra and (d) Cu mapping monograph for SR6 composition after fracture test.

Table 4
Electrical properties of SR composition Specimen.

Specimen	Electrical Resistance (GΩ)
SR1	>200
SR2	>200
SR3	>200
SR4	193.3
SR5	163.8
SR6	141.3

is appropriate to credit the notable reduction in the electrical resistivity of the SR composition with 4% & 8% Graphene filler and 1% of constant CuO filler to the high conductivity of filler content. The SEM images show the uniform distribution of graphene, and this leads to formation of a conductive network due to increased concentration of graphene. Secondly the high aspect ratio of the graphene also contributes to the development of conductive network. Additionally, the free charge carriers cause the Maxwell Wagner-Sillar effect (MSW) which leads to interfacial and electronic polarisation. This helps the easier transfer of electrons which results in the enhanced conductivity as the graphene wt. % is increased.

4. Conclusion

A novel nanocomposite of silicon rubber with graphene/CuO was successfully created. The Graphene/CuO-SR nanocomposite demonstrated exceptional qualities when tested for mechanical and electrical performance, making it suitable for a variety of uses in the various engineering and other industries. Mechanical Properties such as load, hardness, tear, tensile strength and additionally, a FESEM and XRD study of the fractured surfaces was carried out.

The nanocomposite of silicon rubber (SR)-graphene/CuO with 4% weight percentage graphene along with constant rate of CuO at 1% has the greatest values for tensile and tear strengths (SR5). Comparing the tear and tensile strengths to the pure SR1 composition, they both rise by more than 146.52 and 119.77%, respectively. Similarly, Hardness demonstrated consistent improvement as the Graphene/CuO % rose. Whereas the FE-SEM Fracture surface morphology of various configurations supports the findings from the mechanical investigations. For the SR5 composition, the Graphene/CuO distribution is more even and smoother. The development of fundamental analysis of the nanocomposite, which has a wide variety of safe uses, including the technology sector, is supported by the results of the primary study.

Declaration of competing interest

The authors declare that they have no known competing financial interests or personal relationships that could have appeared to influence the work reported in this paper.

Acknowledgement

The authors are grateful for the financial support given by The Ministry of Higher Education Malaysia (MOHE) under the Higher Institution Centre of Excellence (HICOE2.0/5210004) at the Institute of Tropical Forestry and Forest Products. The authors would also like to thank Universiti Putra Malaysia for the financial support through Geran Inisiatif Putra Siswazah (GP-IPS) with grant number 9739200.

References

[1] Ahmed Thabet, Fahad A, Al mufadi. Recent advances in optical characterization of SR/MWCNTs nanostructures for emerging piezoelectric sensors. E-prime - advances in electrical engineering. Electronics and Energy 2024;7:100447. https://doi.org/10.1016/j.prime.2024.100447.

[2] Jin Guangzhi, Lu Yonglai, Peng Yu, Zhang Liqun. Simple method to prepare fluorescent silicon rubber by melt-compounding with crude carbon dots fluid. Mater Today Commun 2021;27:102413. https://doi.org/10.1016/j.mtcomm.2021.102413.

[3] Zhu Chao, Mahmood Zarak, Arshad Abdul Saboor, Jia Liu, Ma Hongrui. Recovery of o-toluidine and p-toluidine from wastewater by silicon rubber membrane extraction. Environmental Technology & Innovation 2020;19:100873. https://doi.org/10.1016/j.eti.2020.100873.

[4] Lai Liangqing, Liu Jia, Lv Zhen, Gao Tianming, Luo Yongyue. Recent advances for flame retardant rubber composites: mini-review. Advanced Industrial and Engineering Polymer Research 2023;6:156–64. https://doi.org/10.1016/j.aiepr.2022.12.002.

[5] Heidarian Atefeh, Naderi-Samani Hamed, Razavi Reza Shoja, Nejad Jabbari Mahsa, Naderi-Samani Ehsan, Gavahian jahromi Mohammad. Study of nickel-coated graphite/silicone rubber composites for the application of electromagnetic interference shielding gaskets. Materials 2024;2:100097. https://doi.org/10.1016/j.nxmate.2023.100097.

[6] Zhou Xinyu, Wang Guangfei, Wang Meimei, Zhang Yu, Yin Wanlei, He Qiang. A simple preparation method for superhydrophobic surface on silicon rubber and its properties. Prog Org Coating June 2020;143:105612. https://doi.org/10.1016/j.porgcoat.2020.105612.

[7] Heidarian Atefeh, Naderi-Samani Hamed, Razavi Reza Shoja, Jabbari Mahsa Nejad, Naderi-Samani Ehsan. Synthesis of nickel particles for use in nickel/silicone rubber composites for the application of electromagnetic interference shielding gaskets. Heliyon 2024;10:e24690. https://doi.org/10.1016/j.heliyon.2024.e24690.

[8] Farahani Atefe, Jamshidi Masoud, Foroutan Masumeh. Improving thermal/electrical properties of silicone rubber nanocomposite using exfoliated boron nitride nano sheets made by an effective/novel exfoliating agent. Mater Des 2023;229:111935. https://doi.org/10.1016/j.matdes.2023.111935.

[9] Gao Mu, Xia Zhidong, Wang Xuelong, Wang Jinshu, Pei Huang. Fabrication of a flexible capacitor sensor with surface-fabric-structured conductive silicon rubber. Sensors and amp; Actuators: A. Physical 2019. https://doi.org/10.1016/j.sna.2019.06.001.

[10] Wanga Xuelong, Xiaa Zhidong, Chen Zhaoa, Pei Huangb, Zhaob Shaofan, Mu Gaoa, Nie Jingkai. Microstructured flexible capacitive sensor with high sensitivity based on carbon fiber-filled conductive silicon rubber. Sensors and Actuators: A. Physical 2020. https://doi.org/10.1016/j.sna.2020.112147.

[11] Goutam Hatui, Asish Malas, Bhattacharya Pallab, Dhibar Saptarshi, Kanti Kundu Mrinal, Das Chapal Kumar. Effect of expanded graphite and PEI-co-Silicon Rubber on the thermos mechanical, morphological as well as rheological properties of in situ composites based on poly (ether imide) and liquid crystalline polymer. J Alloys Compd 2015;619:709–18. https://doi.org/10.1016/j.jallcom.2014.08.144.

[12] Huang Pei, Xia Zhidong, Cui Song. 3D printing of carbon Fiber filled conductive silicon rubber. The address for the corresponding author was captured as affiliation for all authors. Journal of Materials & Design 2017. https://doi.org/10.1016/j.matdes.2017.12.051.

[13] Yin S, Ma L, Wu LZ. Carbon fiber composite lattice structure filled with silicon rubber. Procedia Eng 2011;10:3191–4. https://doi.org/10.1016/j.proeng.2011.04.527.

[14] Hsien T Chiua, Sukachonmakul Tanapon, Wanga Chen H, Wattanakul Karnthidaporn, Kuoa Ming T, Wang Yu H. Effect of pyrolysis atmospheres on the morphology of polymer-derived silicon oxynitrocarbide ceramic films coated aluminum nitride surface and the thermal conductivity of silicone rubber composites. Appl Surf Sci 2014;292:319–27. https://doi.org/10.1016/j.apsusc.2013.11.139.

[15] Meekum Utai, Khiansanoi Apichart. PLA and two components silicon rubber blends aiming for frozen foods packaging applications. Results Phys 2018;8:79–88. https://doi.org/10.1016/j.rinp.2017.11.030.

[16] Singh Upinder Pal, Biswas Bidyut Kumar, Ray Bidhan Chandra. Evaluation of mechanical properties of polypropylene filled with wollastonite and silicon rubber. Mater Sci Eng 2009;501:94–8. https://doi.org/10.1016/j.msea.2008.09.063.

[17] Chen Zhao, Xia Zhidong, Wang Xuelong, Nie Jingkai, Pei Huang, Shaofan Zhao. 3D-printed highly stable flexible strain sensor based on silver-coated-glass fiber-filled conductive silicon rubber. Mater Des 2020;193:108788. https://doi.org/10.1016/j.matdes.2020.108788.

[18] Ouyang Y, Li X, Ding F, Bai L, Yuan F. Simultaneously enhance thermal conductive property and mechanical properties of silicon rubber composites by introducing ultrafine Al $_2O_3$ nanospheres prepared via thermal plasma. Compos Sci Technol 2020. https://doi.org/10.1016/j.compscitech.2020.108019.

[19] Hino Tomoaki, Igarashi Yusuke, Ymauchi Yuji, Nishikawa Masana. Surface wettability of silicon rubber after irradiation with a glow discharge plasma. Vacuum 2009;83:506–9. https://doi.org/10.1016/j.vacuum.2008.04.015.

[20] Chiu Hsien Tang, Sukachonmakul Tanapon, Kuo Ming Tai, Wang Yu Hsiang, Wattanakul Karnthidaporn. Surface modification of aluminum nitride by polysilazane and its polymer-derived amorphous silicon oxycarbide ceramic for the enhancement of thermal conductivity in silicone rubber composite. Appl Surf Sci 2014;292:928–36. https://doi.org/10.1016/j.apsusc.2013.12.081.

[21] Shinde Avinash, Siva I, Munde Yashwant, Sankar I, Sultan Mohamed Thariq Hameed, Mustapha Faizal, Shahar Farah Syazwani, Najeeb Muhammad Imran. The impacts of graphene dosage on the friction and wear performance of a graphene-reinforced silicone rubber nano composite. J Mater Res Technol 2022:1570–80. https://doi.org/10.1016/j.jmrt.2022.10.007.

[22] Seyedmehdi SA, Zhang Hui, Zhu Jesse. Influence of production method, silicone type and thickness on silicon rubber superhydrophobic coatings. Prog Org Coating 2016;90:291–5. https://doi.org/10.1016/j.porgcoat.2015.10.024.

[23] Cheng Li, Liu Yunfan, Cheng Zhidong, Chen Rongxin, Zhang Sida, Liao Ruijin, Yuan Yuan. A novel aging characterization method for silicone rubber based on terahertz absorption spectroscopy. Polym Test 2022;115:107723. https://doi.org/10.1016/j.polymertesting.2022.107723.

[24] Kulkarni Giridhar S, Shivashankar GS, Sudeep kumar T, Vijay kumar BK. Effect of processing parameters on tensile strength of GFRP with liquid silicon rubber and reinforced with fine aluminium powder and silica powder. Mater Today Proc 2017;4:11279–84. https://doi.org/10.1016/j.matpr.2017.09.051.

[25] Li Jingchao, Zhao Xiuying, Wu Wenjie, Ji Xiaowang, Lu Yonglai, Zhang Liqun. Bubble-templated rGO-graphene nanoplatelet foams encapsulated in silicon rubber for electromagnetic interference shielding and high thermal conductivity. Chem Eng J 2021;415:129054. https://doi.org/10.1016/j.cej.2021.129054.

[26] Elsafi M, jamal Alasali Heba, Almuqrin Aljawhara H, Mahmoud KG, Sayyed MI. Experimental assessment for the photon shielding features of silicone rubber reinforced by tellurium borate oxides. Nucl Eng Technol 2023;55:2166–71. https://doi.org/10.1016/j.net.2023.02.022.

[27] Fu Shao-Yun, Feng Xi-Qiao, Lauke Bernd, Wing Mai Yiu. Effects of particle size, particle/matrix interface adhesion and particle loading on mechanical properties of particulate–polymer composites. Composites Part B 2008;39:933–61. https://doi.org/10.1016/j.compositesb.2008.01.002.

[28] Chen Jinhan, Liu Jian, Peng Zhilong, Yao Yin, Chen Shaohua. The microscopic mechanism of size effect in silica-particle reinforced silicone rubber composites. Eng Fract Mech 2021;255(1 October):107945. https://doi.org/10.1016/j.engfracmech.2021.107945.

[29] Javad Azizli Mohammad, Rezaeinia Sheida, Rezaeeparto Katayoon, Mokhtary Masoud, Askari Fahimeh. Enhanced compatibility, morphology, rheological and mechanical properties of carboxylated acrylonitrile butadiene rubber/chloroprene rubber/graphene nanocomposites: effect of compatibilizer and graphene content. RSC Adv 2020;10:11777. https://doi.org/10.1039/d0ra00517g.

[30] Hasanzadeh Kermani Hamed, Mottaghitalab Vahid, Mokhtary Masoud, Alizadeh Omid. Recent advances in carboxylated butadiene rubber nanocomposites: effect of carbon nanotube and graphene oxide. J Polym Res 2022;29:447. https://doi.org/10.1007/s10965-022-03293-y.

[31] Javad Azizli Mohammad, Amin Iranpoury, Barghamadi Mohammad, Rezaeeparto Katayoon, Parham Somayeh, Jahankhah Zahra, Mokhtary Masoud, Hashemi Mohammad. Compatibilization of novel GO-XNBR-g-GMAC/XNBR/XSBR nanocomposites: the relationship between structure and properties. Compos Interfac 2023;30(7):803–26. https://doi.org/10.1080/09276440.2023.2179234.

[32] Javad Azizli Mohammad, Parham Somayeh, Saeed Abbasizadeh, Mokhtary Masoud, Rezaeinia Sheida, Darabi Mehdi Jokeri. Preparation and characterization of carboxylated acrylonitrile butadiene rubber/carboxylated styrene butadiene rubber (XNBR/XSBR) nanocomposites in the presence of dichlorocarbene-modified SBR (DCSBR) compatibilizer and montmorillonite. Polym Bull 2021;78:1637–69. https://doi.org/10.1007/s00289-020-03177-5.

[33] Azizli MJ, Barghamadi M, Rezaeeparto K, et al. Theoretical and experimental analyses of rheological, compatibility and mechanical properties of PVMQ/XNBR-g GMA/XNBR/GO ternary hybrid nanocomposites. Iran Polym J (Engl Ed) 2021;30:1001–18. https://doi.org/10.1007/s13726-021-00953-6.

[34] Shinde Avinash, Siva Irulappasamy, Munde Yashwant, Sankar Irulappasamy, Sultan Mohamed Thariq Hameed, Shahar Farah Syazwani, Gaff Milan, Hui David. Appraising the dielectric properties and the effectiveness of electromagnetic shielding of graphene reinforced silicone rubber nanocomposite. Nanotechnol Rev 2023;12:20220558. https://doi.org/10.1515/ntrev-2022-0558.